Journal of Catalysis **193,** 308–318 (2000)
doi:10.1006/jcat.2000.2902, available online at http://www.idealibrary.com on IDEAL®

Selective Oxidation of *n*-Butane on a V–P–O Catalyst: Study under Fuel-Rich Conditions

S. Mota, M. Abon, J. C. Volta, and J. A. Dalmon

Institut de Recherches sur la Catalyse, 2 Avenue Albert Einstein, 69626 Villeurbanne Cédex, France

Received January 12, 2000; revised April 24, 2000; accepted April 24, 2000

A vanadium pyrophosphate oxide (V–P–O) catalyst has been tested for *n*-butane oxidation under fuel-rich conditions ($O_2/C_4H_{10} = 0.6$). A rapid decrease in maleic anhydride production was observed with time. XPS analysis showed that this was associated with a rapid reduction of the catalyst surface. From the evolution of the distribution of products, it has been inferred that CO formation mainly occurs by the oxidation of adsorbed butane whereas CO_2 is formed by the overoxidation of maleic anhydride. It has been concluded that the *n*-butane activation occurs on V^{4+} sites while the insertion of oxygen in the C_4-intermediates leading to MA takes place on V^{5+} sites. The deactivation in fuel-rich conditions is not so drastic when the V–P–O catalyst has been previously oxidized at a relatively low temperature (500°C). In this case oxygen is stored in the V–P–O surface region, hence favoring the specific O-inserting role of V^{5+} responsible for MA formation.

Key Words: n-**butane partial oxidation; maleic anhydride; fuel-rich feed conditions.**

1. INTRODUCTION

Maleic anhydride has been produced for a long time by the partial oxidation of benzene. The catalyst used has been based on V_2O_5–MoO_3 mixed oxide deposited on a support. The conversion is almost total (97–99%), and the selectivity is near 75% with CO and CO_2 by-products. During the 1980s, *n*-butane partial oxidation was developed for economical (low price and availability of butane) and environmental (toxicity of benzene) reasons (1, 2).

n-Butane catalytic oxidation is still the only example of an industrially performed oxidation reaction of a light alkane. V–P–O catalysts are known to be efficient for the production of maleic anhydride (termed MA) from *n*-butane (1–4). A single $(VO)_2P_2O_7$ phase has been inferred to be present in the long-term activated catalyst (5–7). The catalytic properties of the vanadyl pyrophosphate catalyst depends on the nanostructure and the morphology of the $(VO)_2P_2O_7$ crystals (8). The V^{5+}/V^{4+} dimeric species in the topmost oxidized layer of vanadyl pyrophosphate have been proposed as the active sites (3). Other authors suggest that the active sites lie within microdomains of crystalline vanadyl orthophosphate (V^{5+}) formed on the (100) face of $(VO)_2P_2O_7$ (V^{4+}) crystallites under catalytic reaction conditions (9, 10). It has been also considered that the defects in the (100) face play an important role in the reaction (9).

From an industrial point of view, a distinction is made between a nonequilibrated (short-term catalytic test) and equilibrated (long-term catalytic test) catalyst, and it has been shown that, when working under fuel-lean conditions (C_4H_{10}/air = 1–3%) the catalytic conditions (C_4H_{10}/air mixture, temperature, time) tend to change the V^{5+}/V^{4+} ratio in such a way that the oxidation rate of V^{4+} to V^{5+} will be decreasing for the equilibrated catalyst (11). It has been pointed out that this specific point requires further investigation since the catalytic performances are directly connected to the changes occurring in the V–P–O catalyst during activation and aging (11). The surface of the V–P–O catalyst is progressively reduced with time-on-stream as observed by XPS (12). When increased C_4/air ratios are used, it is possible to detect the formation of olefinic intermediates (butenes, butadiene) from *n*-butane. In this case, V^{3+} species are detected in the catalysts (13).

In industry, different types of reactors have been considered for this catalytic reaction (14), fixed-bed (15, 16), fluidized-bed (17), and recirculating solid (18, 19) reactors. The fixed-bed reactor is a multiple tube heat exchanger reactor. Under industrial conditions with 2% *n*-butane in the feed, conversions range from 70 to 85% with a molar selectivity to MA of around 67–75% (1). In a fluidized-bed reactor, the reaction gases flow upward through a bed of fine catalyst particles. This system offers the advantage of operating at higher butane concentrations (up to 4%), thus lower operating costs. The recirculating solid reactor developed by DuPont de Nemours (17–19) allows the rapid recycling of the V–P–O solid thanks to a high gas velocity. In this reactor, the oxidation of *n*-butane over the oxidized V–P–O catalyst and the regeneration (oxidation) of the reduced V–P–O catalyst are performed in separate zones. This configuration results in an increase of the selectivity to MA (up to 90%) (19), because the oxidation state of the catalyst is optimized. Since the reduction stage occurs separately, a more concentrated *n*-butane stream can be used.

0021-9517/00 $35.00

However, these different types of reactors present some disadvantages. In the fixed-bed, due to the exothermicity of the reaction, the extent of the reaction must be limited in order to avoid the formation of hot spots and the possibility of explosive mixtures. For the fluidized-bed reactor and the recirculating fluidized-bed reactor, the major constraint is the attrition resistance of the catalyst. Furthermore in the latter, large amounts of catalyst have to be recirculated from the reactor to the regenerator. In conclusion, whatever the type of reactor, the maleic anhydride yield in industrial processes is below 60%.

In order to improve the maleic anhydride yield, it has been proposed that researchers work with a high *n*-butane concentration and a low O_2/C_4H_{10} ratio (fuel-rich conditions) to limit total oxidation (13, 20, 21). By comparing the effect of butane concentration on maleic anhydride selectivity, Centi *et al.* (20) showed that decreasing the oxygen concentration from 20 to 5% vol at 1.5% vol of *n*-butane led to a 5% increase in the maximum yield of maleic anhydride (from 51 to 56%) in the reaction range from 300 to 340°C. In another study, also performed under fuel-rich conditions, Hutchings showed that it is possible to achieve a higher MA selectivity (80 mol%) at 9% butane conversion (21) with a feed composition of 20.3 mol% butane, 18.9 mol% oxygen at 360°C and a GHSV of 1000 h^{-1}. Furthermore, even with a low *n*-butane conversion per pass, the exit gas contained significantly higher MA concentrations (1.5–2.0 mol%) than under conventional fuel-lean operating conditions. In this way, substantial yield can be recovered by condensation rather than by using the conventional water scrubbing recovery technique. However, operating under fuel-rich conditions necessitates a recycling process (21).

We are presently developing a new type of reactor based on a ceramic porous tubular membrane. The V–P–O catalyst will be placed as a fixed bed in the inner volume of the tube. Butane will be directly fed at the inlet of the tube, and oxygen will be gradually distributed from the shell side along the tube. The membrane allows control of the oxygen supply to the catalyst bed, and in this case a low, constant partial pressure of O_2 can be thus maintained on the catalyst. It is anticipated that this feature will improve the maleic anhydride selectivity by limiting the total oxidation reaction. This membrane reactor concept has already been proposed for various selective oxidation processes (oxidative coupling of methane, oxidation of ethylene to acetaldehyde and of propene to acrolein) (22). Moreover, the ability to distribute the oxygen feed through a membrane may allow a better management of the heat produced and also the use of global oxygen/hydrocarbon ratios corresponding to explosive mixtures in conventional reactors (23). Due to its geometry (the oxygen partial pressure is kept low but constant along the fixed bed, when the *n*-butane concentration is decreasing progressively through conversion), the membrane reactor will operate with a continuous change of the O_2/C_4H_{10} ratio, from fuel-rich conditions at the inlet of the reactor to oxygen-rich at the outlet. Therefore, the implementation of this membrane reactor requires a catalyst able to work under conditions where reactants are fed with different ratios.

The present work has been performed in a conventional fixed-bed reactor. The performance of a standard V–P–O catalyst has been investigated as a function of the composition of the reactant gas mixture (O_2/C_4H_{10} ratio). In order to simulate the reducing conditions prevailing in the beginning of the catalytic bed of the membrane tubular reactor, a fuel-rich mixture was fed. A specific oxygen-pretreatment of the V–P–O catalyst has been considered in order to adapt the solid to this reducing atmosphere. Indeed it was previously observed that such a pretreatment improved the selectivity to maleic anhydride under conventional fuel-lean conditions (25, 26).

2. EXPERIMENTAL

2.1. Catalyst Preparation

The precursor, $VO(HPO_4)$,$0.5\,H_2O$ was prepared according to the method given by Johnson *et al.* (28). V_2O_5 (11.8 g) was added to isobutanol (250 ml) and refluxed with H_3PO_4 (85%) for 16 h. The blue suspension was then separated from the organic solution by filtration and washed with isobutanol and ethanol. The resulting solid was refluxed in water, filtered hot and dried in air at 110°C for 16 h.

Pellets from the fine powder of precursor was made using 3.4% graphite, giving cylindrical particles of 6 mm diameter and ca. 8 mm length.

In order to obtain the $(VO)_2P_2O_7$ catalyst, hereafter denoted PYRO, the precursor was calcined under N_2 at 550°C for 72 h.

2.2. Oxidizing Pretreatment

The PYRO catalyst (ca. 0.5 g) was heated to 500°C (5°C/min) under a flow of oxygen (20 ml/min) and then kept at this temperature for 2 h. This procedure follows that proposed by Aït Lachgar *et al.* (25). The resulting solid was denoted PYRO.OX.

2.3. Experimental Setup

The catalytic experiments were carried out in a fixed-bed reactor at atmospheric pressure. The reactor, a classical tubular Pyrex microreactor, was equipped with a thermocouple inside the catalytic bed for continuous temperature control. Five hundred milligrams of catalyst was commonly used.

Sampling valves were inserted in a hot box heated at 150°C to avoid condensation of maleic anhydride. The flow of gas reactants was regulated by mass flow controllers. The feed consisted of a mixture of *n*-butane, oxygen, and helium.

The reaction was carried out at 400°C with a total flow rate of 25 cm^3 min^{-1} and at a constant GHSV of 3000 h^{-1}.

Two different feed compositions were chosen:

—Standard oxidizing conditions: $O_2/C_4 = 12$ corresponding to $C_4/O_2/He = 0.8:10:92$ to mimic the situation at the outlet of the catalytic bed in the membrane reactor.

—reducing conditions: $O_2/C_4 = 0.6$ corresponding to $C_4/O_2/He = 16.6:10:73.4$ to mimic the situation at the inlet of the catalytic bed in the membrane reactor. This low value has been roughly estimated as that existing in the first tenth of a tubular zeolite membrane acting as oxygen distributor in the catalyst bed. It has been calculated on the basis of the O2 permeance of the zeolite membrane (24) and a ratio (total distributed) of O2/C4 of 12. Oxygen feed has been kept constant.

Reactants and reaction products were analyzed by on-line gas chromatography using double FID detection (HP5890A series II) with HP-PLOT/Al_2O_3 (C_4H_{10}) and HP-INNOWAX (MA) columns followed by a TCD detector (Intersmat GC IGC 120 MB) with a CTR1 column (O_2, CO, CO_2). A computer was used with HP Chemstation software.

2.4. Catalyst Characterization

The specific surface area of the samples was measured by the BET method with N_2 adsorption at 77 K automatically controlled by volumetry with a homemade apparatus.

X-ray diffraction (XRD) patterns were collected with a Siemens D500 diffractometer using Cu $K\alpha$ radiation.

The ^{31}P NMR spectra were recorded with a Bruker DSX400 spectrometer at 161.9 MHz, equipped with a standard 4-mm probe head. The ^{31}P Spin Echo Mapping (SEM) spectra were obtained with a sweep width of 2 MHz, $t = 20$ μs, and a 90° pulse length of 1.5 μs. The ^{31}P MAS spectra were recorded at 12 kHz spinning speed with a P/2 acquisition sequence, a pulse length of 1.5 μs, and a recycle delay of 60 s.

XPS analysis was performed in a VG Escalab 200R machine using Mg $K\alpha$ radiation. The electrical charge was corrected by setting the binding energy (BE) of adventitious carbon (C_{1s}) at 284.5 eV. For quantitative analysis, the integrated area under $V_{2p3/2}$, O_{1s}, P_{2p}, and C_{1s} peaks after smoothing and subtraction of a nonlinear Shirley background was used. Analysis of the $V_{2p3/2}$ level allowed us to measure the changes in the surface oxidation state of vanadium (V^{5+}, V^{4+}, and V^{3+}) from a peak decomposition and curve fitting technique, as already described (12).

3. RESULTS

3.1. Catalytic Results under Standard Feed Conditions ($O_2/C_4 = 12$)

Table 1 compares the catalytic performance of the PYRO catalyst before and after an oxidizing pretreatment.

TABLE 1

Catalytic Performance of PYRO and PYRO.OX Catalysts under Standard Feed Conditions

Catalyst	$C(C_4H_{10})$	$C(O_2)$	S(MA)	$S(COx)$	Y(MA)
PYRO	20	6	76	22	15.2
PYRO.OX	12	1	91.4	8.6	10.9

Note. $O_2/C_4 = 12$; GHSV = 3000 h^{-1}; $T = 400$°C. $C(C_4H_{10})$ and $C(O_2)$: *n*-butane and oxygen conversions. S(MA) and $S(COx)$: selectivity for MA and CO*x*. Y(MA): MA yield.

PYRO.OX was more selective (S(MA) = 91.4% instead of 76%) but with a lower conversion (12% instead of 20%). With increasing MA selectivity, the formation of CO*x* decreased, particularly for CO_2. Note that these catalytic results are stable with reaction time, at least for 24 h (duration of the run).

3.2. Catalytic Results under Reducing Feed Conditions

In order to be near the feed conditions for the first catalyst layer of the membrane reactor, both catalysts, PYRO and PYRO.OX, were tested with an excess of butane ($O_2/C_4 = 0.6$), i.e., under fuel-rich conditions.

Figures 1a and 1b show the changes in the catalytic performance of the PYRO catalyst as a function of time.

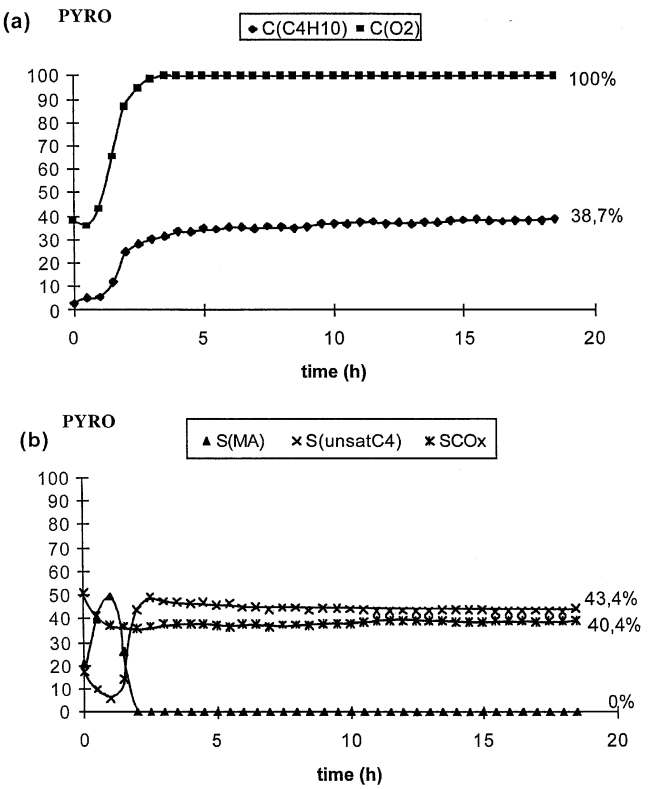

FIG. 1. Catalytic performance of PYRO catalyst under reducing feed conditions ($O_2/C_4 = 0.6$), $T = 400$°C: (a) conversions, $C(C_4H_{10})$ and $C(O_2)$; (b) selectivities, S(MA), S(unsatC_4), and $S(COx)$.

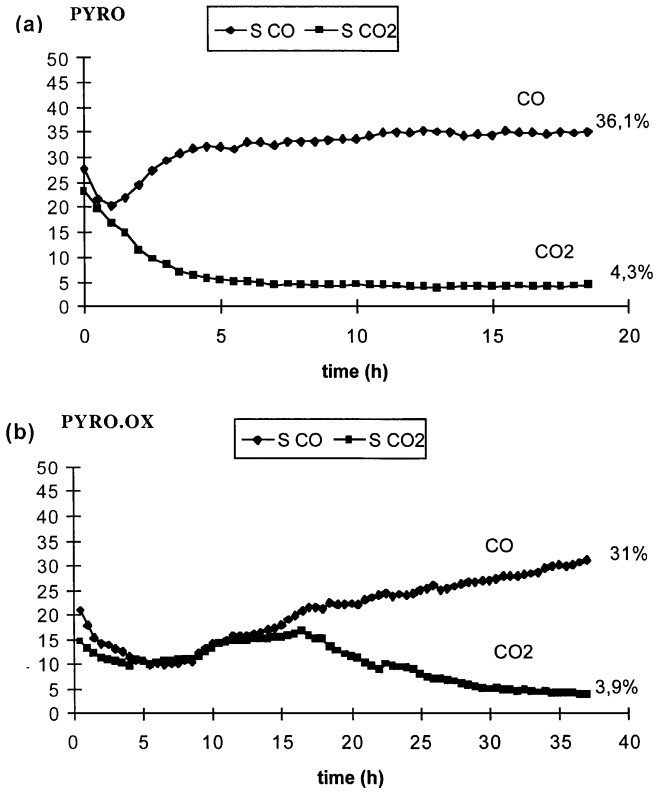

FIG. 2. CO and CO_2 selectivities for PYRO (a) and PYRO.OX (b) catalysts under reducing feed conditions ($O_2/C_4 = 0.6$), $T = 400°C$.

Butane and oxygen conversions (Fig. 1a) first increased rapidly to reach a steady state, $C(C_4H_{10})$ from 2.8 to 38.7% and $C(O_2)$ from 38.4 to 100%. MA selectivity (Fig. 1b), reached a maximum $S(MA) = 49.4\%$ after 1 h on stream; then $S(MA)$ dropped to zero after 2 h on stream. Conversely, the selectivity for unsaturated C_4 (1-butene, *cis*-2-butene, *trans*-2-butene), low at the beginning of the reaction ($S(\text{unsat}C_4) = 17.5\%$ at $t = 0$ and 7% at $t = 1$ h), sharply increased later on ($S(\text{unsat}C_4) = 51.2\%$ at $t = 2$ h).

Figure 2a describes the evolution of CO and CO_2 as a function of time for the PYRO catalyst. CO and CO_2 selectivities were similar (respectively, 21.6 and 19.7%) during the first hour on stream, then $S(CO_2)$ decreased to 4.3%, while $S(CO)$ increased up to 36.1% at steady state (18 h). Consideration of the carbon balance, which is 83.8% at steady state, shows that there is a deposit of carbonaceous polymeric species at the surface of the catalyst. This has been confirmed by the formation of CO*x* when the used catalyst (at the end of the test) was treated under an oxygen flow at 400°C. The evolution of the different selectivities for unsatC_4 are shown in Fig. 3a. At the beginning of the reaction, the total unsatC_4 selectivity is low (Fig. 1b, 17.5% at $t = 0$ and 6% at $t = 1$ h) and no differences between their distribution could be noticed. However, after 18 h on stream, there was a significantly different distribution: 1-butene selectivity increased strongly (24.2%); *cis*-2- and *trans*-2-butenes were produced in similar amounts (respectively, 7.1 and 10.5%), and selectivity toward butadiene was low (2.5%). The steady state was reached after 7 h on stream: the PYRO catalyst was equilibrated and its performances remained stable: $C(C_4H_{10}) = 38.7\%$, $C(O_2) = 100\%$, $S(MA) = 0\%$, $S(\text{unsat}C_4) = 43.4\%$, and $S(CO_x) = 40.4\%$. All the oxygen present in the gaseous phase is consumed and therefore the surface of the catalyst is most likely reduced. This should be the reason for the formation on unsaturated C_4 and the absence of maleic anhydride (12). In Fig. 3b, the different selectivities for butenes have been normalized with respect to the selectivity for *cis*-2-butene. This figure will be discussed later.

Figures 4a and 4b show the variation of the PYRO.OX catalytic performances under the same feed conditions as before. From these results, we observed that the PYRO.OX behaved similarly to the PYRO catalyst when compared with Fig. 1, but over a different time scale: the steady state for PYRO.OX catalyst was reached only after 25 h. The C_4H_{10} and O_2 conversions increased more slowly, and the catalyst remained selective to mild oxidation for a longer time (almost 10 h): $S(MA)$ goes first to a maximum (64.2% at $t = 5$ h) and then decreases to zero after 15 h of run. At steady state, the catalytic performances were close to those of the PYRO catalyst: $C(C_4) = 38.5\%$, $C(O_2) = 100\%$,

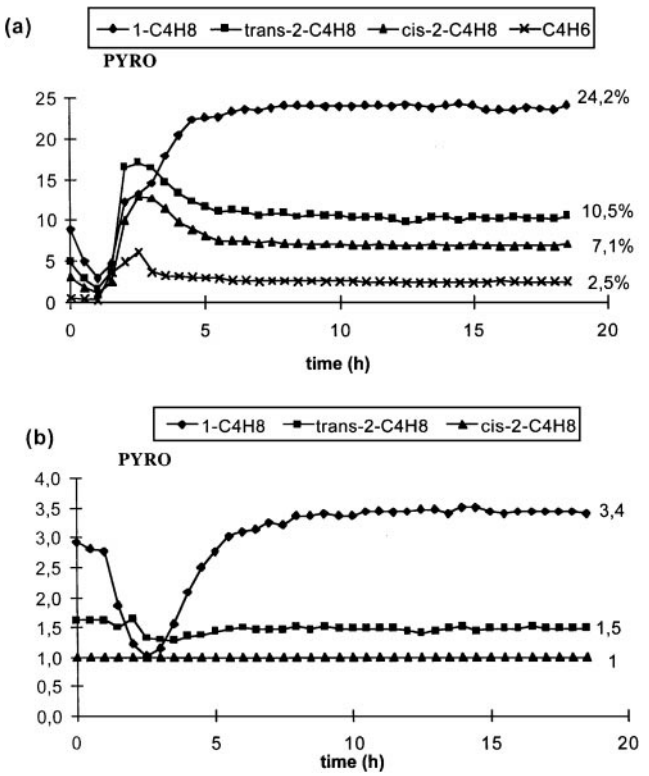

FIG. 3. Unsaturated-C_4 selectivities (a) and normalized butene selectivities (b) (as refered to *cis*-2-C_4H_8) for PYRO catalyst under reducing feed conditions ($O_2/C_4 = 0.6$), $T = 400°C$.

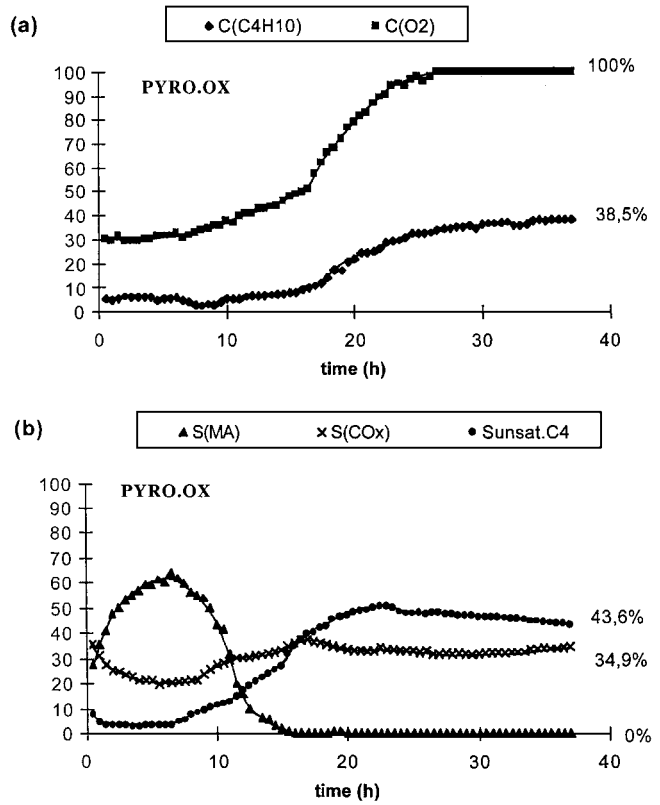

FIG. 4. Catalytic performance of PYRO.OX catalyst under reducing feed conditions ($O_2/C_4 = 0.6$), $T = 400°C$: (a) conversions, $C(C_4H_{10})$ and $C(O_2)$; (b) selectivities, $S(MA)$, $S(\text{unsat}C_4)$, and $S(COx)$.

$S(MA) = 0\%$, $S(\text{unsat}C_4) = 43.6\%$, and $S(COx) = 34.9\%$. Concerning COx (Fig. 2b), it appears that the selectivities for CO and CO_2 exhibit the same trends for the first 12 h on stream. This goes in parallel with the production of MA while the increase of CO after 12 h when CO_2 decreases may be associated with the production of unsaturated C_4 as previously observed for the PYRO catalyst.

Figure 5a shows the evolution of the selectivities for unsaturated C_4 with time-on-stream. Up to 15 h, butenes were produced in same amount. At 37 h, 1-butenes reached 23.3%, *cis*-2- and *trans*-2 butenes reached 7.4 and 10.6%, respectively, and, finally, butadiene reached 2.3%, values similar to those of the PYRO catalyst. However the kinetics necessary to reach the steady state are different. In Fig. 5b, the different selectivities for butenes have been normalized with respect to the selectivity for *cis*-2-butene. This figure will be discussed later.

The production of maleic anhydride does occur for a longer period under fuel-rich conditions in the case of PYRO.OX (15 h) as compared to PYRO (2 h). This observation suggests that the oxidizing pretreatment has stored oxygen species active in selective oxidation within the V–P–O surface region. This conclusion has been supported by the following physico-chemical investigations.

3.3. Characterization of the Catalysts

3.3.1. XRD. Figure 6 compares the XRD spectra of the PYRO catalyst (a), the PYRO.OX before (b) and the PYRO after (c) test under fuel-rich conditions. The pattern of PYRO (Fig. 6a) is characteristic of the $(VO)_2P_2O_7$ phase with the characteristic (200), (024), and (032) reflections. The reflection at 26.5° (2θ) corresponds to graphite, which has been added for pelletizing the catalyst.

The spectrum of PYRO.OX (Fig. 6b) is also typical of a poorly crystallized $(VO)_2P_2O_7$ phase, which displays a more disorganized structure as compared to PYRO (Fig. 6a). This is obvious from a decrease of the intensity of the diffraction peaks and an increase of the background. It can also be stressed that there are no characteristic lines of any $VOPO_4$ (V^{5+}) phase which could have been formed during the PYRO oxidation. These observations are in agreement with previous results obtained when oxidizing a PYRO catalyst prepared at a higher temperature (750°C) (25) and therefore likely to be less prone to oxidation following O_2 pretreatment at 500°C. The XRD spectrum of PYRO.OX is almost not changed by the test under fuel-rich conditions (compare Figs. 6b and 6c). This catalyst remains, then, as poorly crystallized as before the test.

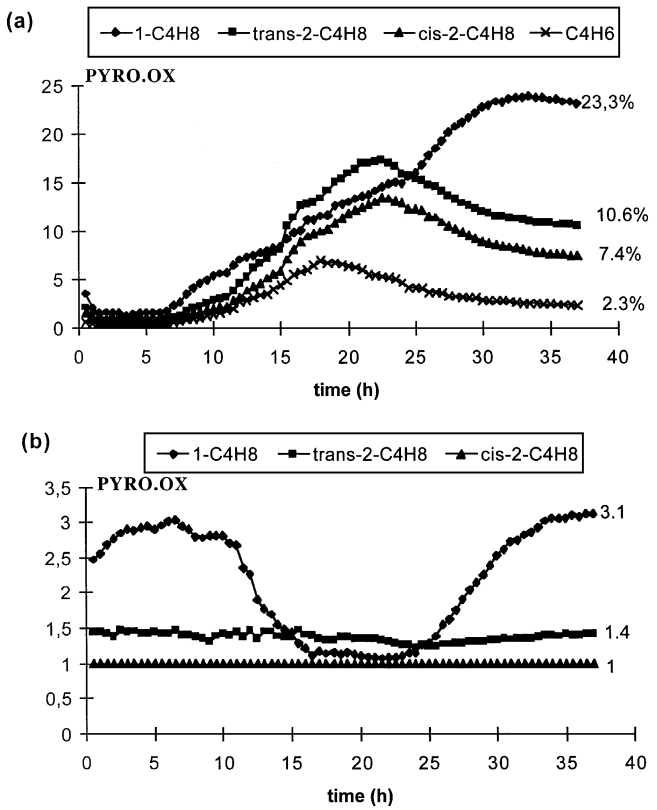

FIG. 5. Unsaturated-C_4 selectivities (a) and normalized butene selectivities (b) (as refered to *cis*-2-C_4H_8) for PYRO.OX catalyst under reducing feed conditions ($O_2/C_4 = 0.6$), $T = 400°C$.

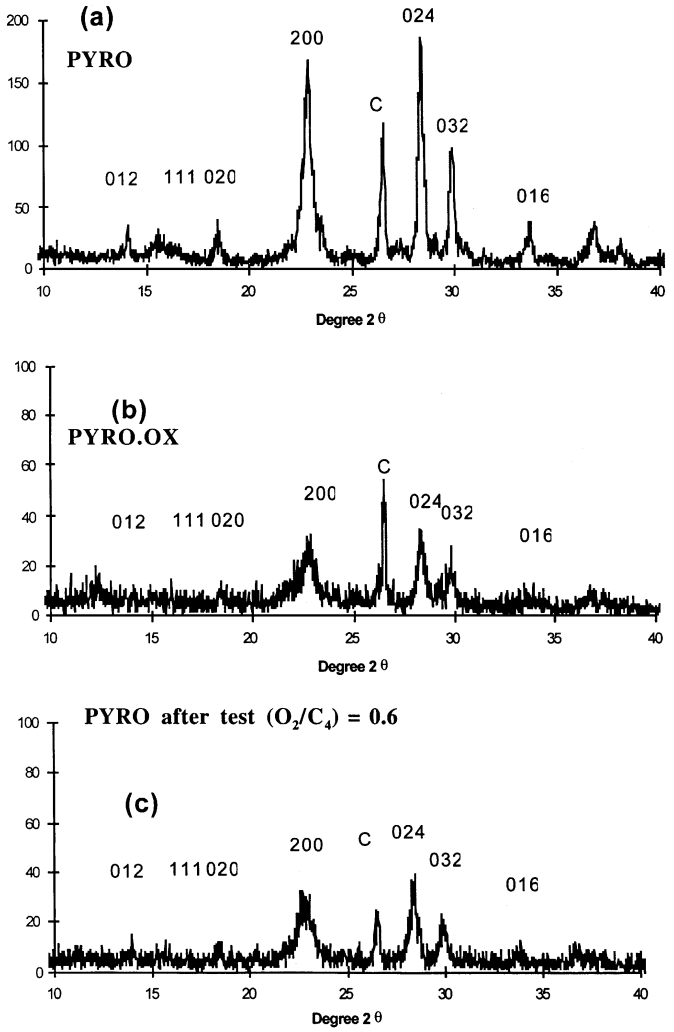

FIG. 6. XRD spectra. Main characteristic $(VO)_2P_2O_7$ lines are indexed. The line at 26.5°2θ corresponds to graphite added for pelletizing: (a) PYRO catalyst; (b) PYRO.OX catalyst; (c) PYRO.OX catalyst after test under fuel-rich conditions.

3.3.2. ^{31}P NMR. Figure 7 compares the Spin Echo Mapping spectra of PYRO (Fig. 7a) and PYRO.OX (Fig. 7b) catalysts. The spectra obtained with the used catalysts after the test under reducing conditions are shown in Figs. 7c and 7d for the PYRO and the PYRO.OX catalysts, respectively.

The PYRO spectrum (Fig. 7a) shows a main peak at 2472 ppm characteristic of $(VO)_2P_2O_7$. This peak position is typical of P atoms in a poorly crystallized $(VO)_2P_2O_7$ phase (12, 25, 26). Recall that a more crystallized $(VO)_2P_2O_7$ exhibits a peak around 2600 ppm (25, 29). The lack of any signal around 0 ppm indicates that the total V^{5+} concentration is very low and impossible to detect by this technique, which is bulk sensitive. Note, however, a small contribution in the 1000-ppm range which has been previously attributed to V^{4+}–V^{5+} pairs (12) since this contribution is never observed on pure $(VO)_2P_2O_7$ samples (26).

The PYRO.OX spectrum (Fig. 7b) shows a displacement of the peak characteristic of $(VO)_2P_2O_7$ from 2472 to 2500 ppm, indicative of a better organization of the material due to the O_2 pretreatement. The intensity of the corresponding peak decreases. An important peak appears around 0 ppm, which corresponds to a significant percentage of P bonded to V^{5+} centers, which illustrates the fact that the PYRO catalyst has been effectively oxidized. The ^{31}P NMR MAS spectrum of the corresponding catalyst (Fig. 7e) shows a band at −13.4 ppm with a broad spinning side band pattern. In a previous publication (26), this signal has been attributed to species characteristic of isolated V^{5+} microdomains located at the surface of the (100) faces of $(VO)_2P_2O_7$ crystallites.

The spectra of PYRO and PYRO.OX after the catalytic test under fuel-rich conditions are both very similar. They are typical of P atoms surrounded by V^{4+} in a poorly crystallized $(VO)_2P_2O_7$ phase. All V^{5+} coming from the V^{4+}–V^{5+} dimers (for PYRO) and from isolated V^{5+} species (for PYRO.OX) have been consumed during the catalytic test. Note also the absence of any signal around 4600–4700 ppm,

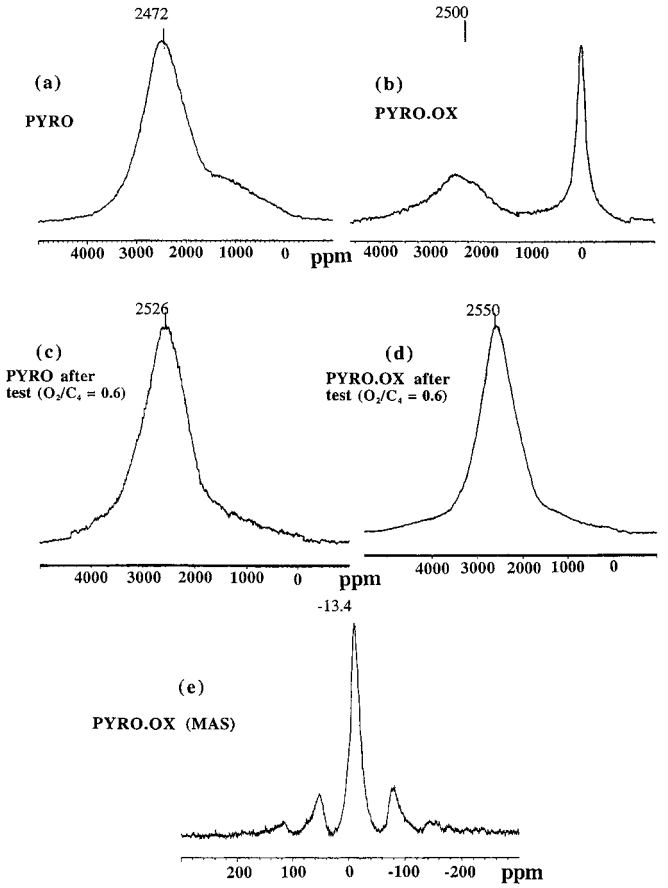

FIG. 7. ^{31}P NMR spectra: (a) spin echo mapping (SEM) of PYRO; (b) SEM of PYRO.OX; (c) SEM of PYRO; (d) SEM of PYRO.OX after reducing feed conditions; (e) magic angle spinning of PYRO.OX.

indicative of the absence of V^{3+} species (25), which should have been developed by the test under fuel-rich reducing conditions. Then the reduction only affects the V^{5+} sites and stops at V^{4+} oxidation.

3.3.3. XPS. Table 2a compares the superficial concentrations of V, P, O, and C measured on both PYRO and PYRO.OX catalysts before and after reaction under fuel-rich conditions.

The C observed on the PYRO and PYRO.OX (fresh catalysts) corresponds to graphite, which has been added for pelletizing. The O_2 pretreatment involves a decrease of the superficial C content due to oxidation. In contrast, the catalytic test under fuel-rich conditions is associated with a strong superficial C deposit as it is observed on both PYRO and PYRO.OX after reaction. In order to follow only the relative superficial distribution of V, P, and O, the relative percentages have been recalculated without the carbon content (values in parentheses in Table 2a). It appears that these percentages do not change for PYRO and PYRO.OX. The main evolution principally concerns the composition after reaction: V strongly decreases from 12.5% down to 10.7% for PYRO and from 12.2% down to 9.3% for PYRO.OX when O moderately increases from 66.4% up to 68.2% for PYRO and strongly increases from 67.1% up to 71.5% for PYRO.OX. This evolution does not affect the superficial composition of P, which almost does not change (21.0% as compared to 21.1% for PYRO and 20.6% as compared to 19.2% for PYRO.OX). The decrease of the V percentage and the increase of the O percentage have to be considered in parallel with the strong increase of the carbon content: indeed, the catalytic test under fuel-rich conditions results in a high deposition of carbonaceous species at the surface of the PYRO and PYRO.OX catalysts. This is responsible for a progressive masking of the active vanadium species which results in a decrease of the V percentage. The carbonaceous species could be polymeric organic chains enriched in oxygen, and, as a consequence, this could be the reason for the increase of the oxygen percentage.

TABLE 2a

Quantitative Analysis in Percentages of V, P, O, and C on the Catalyst Surface by XPS

Catalyst	% V	P	O	C
PYRO (fresh catalyst)	9.4 (12.5)[b]	5.8 (21.1)	49.8 (66.4)	25
PYRO (after reaction)[a]	5 (10.7)	9.8 (21.0)	31.8 (68.2)	53.4
PYRO.OX (fresh catalyst)	10.8 (12.2)	(18.1)	59 (67.1)	12.2
PYRO.OX (after reaction)[b]	3.5 (9.3)	7.2 (19.2)	26.8 (71.5)	62.5

[a] At $T = 400°C$ and $O_2/C_4H_{10} = 0.6$ after 20–40 h working.

[b] Values in parentheses correspond to the atomic percentages when considering only V, P, and O.

TABLE 2b

Estimation of the Relative Percentages of Surface V^{4+} and V^{5+} by XPS

Catalyst	% V^{4+}	V^{5+}	V^{4+}/V^{5+}
PYRO (fresh catalyst)	41	59	0.7
PYRO (after reaction)[a]	72	28	2.6
PYRO.OX (fresh catalyst)	—	100	—
PYRO.OX (after reaction)[a]	75	25	3

[a] At $T = 400°C$ and $O_2/C_4H_{10} = 0.6$ after 20–40 h working.

The $V_{2p3/2}$ peak may be decomposed into two peaks with a binding energy of 518.0 eV for V^{5+} and 516.9 eV for V^{4+} (12). There is no evidence for any V^{3+} contribution at 515.7 eV (Table 2b), in agreement with the absence of these entities as observed with ^{31}P NMR by spin echo mapping. The relative amounts of the V^{4+} and V^{5+} species are given in Table 2b. Note that only the presence of V^{5+} is detected on the fresh PYRO.OX catalyst. After reaction under fuel-rich conditions, there is a strong reduction of V^{5+} to V^{4+} and the vanadium oxidation state is almost identical for the two catalysts, about 75% V^{4+} and 25% V^{5+}.

4. DISCUSSION

Figures 1 and 4 show that the reaction under fuel-rich conditions (O_2/n-$C_4H_{10} = 0.6$) induced dramatic changes in the catalytic performance on both the PYRO and the PYRO.OX catalysts. Let us first discuss the changes in the conversion of the reactants (Figs .1a and 4a).

The initially low *n*-butane conversion increased with the time of reaction and then stabilized at the same level (about 38%) for both the PYRO and the PYRO.OX catalysts. However, these changes were rapid for PYRO (about 5 h) but were much slower (about 25 h) for PYRO.OX. As also proposed in previous studies (25, 26, 29), ^{31}P-NMR (Fig. 7b) and XPS (Table 2b) showed that the PYRO.OX catalyst accumulated a reservoir of active lattice oxygen bonded to V^{5+} species. A reduction of V^{5+} to V^{4+} occurs as evidenced by ^{31}P-NMR (Figs. 7a to 7d) and XPS (Table 2b). XPS and ^{31}P-NMR analysis performed after reaction have shown that the vanadium oxidation state in the PYRO and the PYRO.OX samples is identical, and this observation fits with the same conversion (about 38%) measured at steady state for the two samples.

The consumption of oxygen (Figs. 1a and 4a) during the course of the reaction followed the same trend on both PYRO and PYRO.OX catalysts. As already stated, the

TABLE 3

Steady-State Intrinsic Activities in mol m^{-2} h^{-1} (Calculated for the Same *n*-Butane Partial Pressure) of the PYRO and PYRO.OX Catalysts Working in an Oxidizing ($O_2/C_4 = 12$) or a Reducing ($O_2/C_4 = 0.6$) Gas Mixture

O_2/C_4H_{10}	12	0.6
PYRO	$4.6 \cdot 10^{-5}$	$9.2 \cdot 10^{-5}$
PYRO.OX	$3.7 \cdot 10^{-5}$	$12.6 \cdot 10^{-5}$

difference in the time scales of reduction must be related to the storage of lattice oxygen (created by the oxygen treatment at 500°C) in the PYRO.OX sample. It is quite striking to observe that the activity of both samples at first increases substantially in parallel with the reduction of V^{5+} to V^{4+}. Furthermore the steady state *n*-butane conversion stays high even though the reaction is limited by oxygen supply (100% oxygen consumption), and in spite of important carbon deposits as shown by XPS analysis (Table 3).

It is interesting to compare the steady-state intrinsic activity of the PYRO and PYRO.OX catalysts working either under the standard (oxidizing) conditions (Table 3) or under reducing conditions (Figs. 1 and 4). The comparison is not straightforward since, in order to change the (O_2/*n*-C_4H_{10}) ratio, the *n*-butane partial pressures were very different under the two experimental conditions. However, as stressed by Centi *et al.* (1), most kinetics studies agree on a nearly first-order reaction with respect to the *n*-butane partial pressure. Assuming this first-order rate, the intrinsic steady-state activities under reducing conditions have been calculated in Table 4 for the same *n*-butane partial pressure used under standard conditions. For a given feed condition (O_2/C_4H_{10} ratio), the two catalysts display about the same steady-state activity. This observation may be explained by the leveling effect exerted by the reaction mixture on the degree of oxidation and the surface state of the catalyst. However, the catalyst working for a long time in a reducing atmosphere becomes roughly twice more active than the same catalyst working in an oxidizing atmosphere. Therefore, the present results do support the idea that the activation of *n*-butane occurs on V^{4+} sites, as already proposed in several studies (13, 31–33). Indeed the reaction (the *n*-butane conversion) readily occurs as soon as the alkane is activated. Furthermore, the activation step likely requires a limited number of active V^{4+} sites, possibly a single V^{4+} species, and is therefore not very sensitive to the formation of carbonaceous deposits which are expected to poison the vanadium surface sites.

TABLE 4

Catalytic Results for PYRO.OX after Different Regeneration Steps

O_2/C_4H_{10}	$C(C_4H_{10})$	$C(O_2)$	S(MA)	$S(C_4H_8)$	$S(COx)$
$0.6^{(1)}$	38.5	100	0	43.6	34.9
$12^{(1)}$	29.9	12.2	58.8	0	36.8
$0.6^{(2)}$	38.3	100	0	47.9	30.6
$0.6^{(3)}$	8.9	37.4	41.7	14.9	39.2

Note. $C(C_4H_{10})$ and $C(O_2)$: *n*-butane and oxygen conversions. S(MA), $S(C_4H_8)$, and $S(COx)$: selectivity for MA and CO*x*. The steps are as follows. (1) $O_2/C_4H_{10} = 0.6$: PYRO.OX results after 25 h of run, $O_2/C_4 = 0.6^{(1)}$. (2) $O_2/C_4H_{10} = 12$: reduced PYRO.OX results under fuel-lean conditions, $O_2/C_4 = 0.6^{(1)} \rightarrow 12^{(1)}$. (3) $O_2/C_4H_{10} = 0.6$: PYRO.OX results after reducing–oxidizing–reducing cycle, $O_2/C_4 = 0.6^{(1)} \rightarrow 12^{(1)} \rightarrow 0.6^{(2)}$. (4) $O_2/C_4H_{10} = 0.6$: reduced PYRO.OX reoxidized under pure O_2 and after 2 h of run ($O_2/C_4 = 0.6$), $O_2/C_4 = 0.6^{(1)} \rightarrow 12^{(1)} \rightarrow 0.6^{(2)} \rightarrow O_2$ 500°C 2 h $\rightarrow O_2/C_4 = 0.6^{(3)}$.

As reducing conditions yield a more active catalyst, they also change the selectivity pattern and suppress selective oxidation to MA (Figs. 1b and 4b). Apart from the reducing atmosphere, the total consumption of oxygen may also contribute to the complete drop of MA formation. The oxygen pretreatment at 500°C was quite advantageous since the formation of MA on the PYRO.OX catalyst was observed for about 15 h (Fig. 4b) compared to only 2 h on the PYRO catalyst (Fig. 1b). This is again in agreement with the idea that the storage of active lattice oxygen is associated with selective V^{5+} species in the surface region of the PYRO.OX catalyst. These observations support the view that the presence of selective V^{5+} species is crucial for the oxygen-insertion reaction steps which lead to MA formation, as previously proposed (26, 27, 30, 33–35). Besides their number, the nature of V^{5+} species is also important since most orthophosphate phases are known to be very poorly selective (33, 36, 37). In this respect, it is worth recalling that, in the present work, XRD analysis does not detect the formation of any crystalline $VOPO_4$ phases even after the oxygen pretreatment at 500°C; however, NMR studies do show the presence of V^{5+} species (Fig. 7b). With respect to MA selectivity, Figs. 1b and 4b show a very interesting feature. MA selectivity first increases with time-on-stream, goes through a maximum, and then drops to zero. This phenomenon has been observed previously (26) and clearly illustrates the model developed by Cavani *et al.* (38) explaining that MA selectivity goes through a maximum for a suitable V^{5+}/V^{4+} balance. For the oxidized sample, the V^{5+}/V^{4+} ratio is first too high and therefore the MA selectivity steadily increases with the course of the reaction (favoring the reduction of V^{5+}) for about 7–8 h up to a maximum (about 65%) before slowly decreasing down to zero. One would expect then the absence of V^{5+} species on the surface at this stage. However, XPS analysis still shows the presence of a significant amount of V^{5+} (24–28%) (Table 2). This puzzling observation could be explained by the fact that the whole multistep mechanism leading to the formation of MA demands several adjacent sites (39–41),

known to be vanadium dimers. XPS shows (Table 2) that the presence of carbonaceous deposits were favored under the reducing conditions. These deposits are expected to mask the V^{5+} sites located in the surface. Hence, oxidation to MA (41) would be stopped at the first step (formation of butenes and CO*x*) insofar as the probability of finding free ensembles of selective V^{5+} sites becomes too low.

It is indeed striking to observe that unsatC_4 are the main products when the reaction reaches a steady state under fuel-rich conditions (Figs. 1b and 4b). This is in agreement with Centi *et al.* (14) and Busca (42), who claimed that $(VO)_2P_2O_7$ is substantially an oxidative dehydrogenation catalyst that also contains active sites to insert oxygen. In the present case, the V^{5+} sites responsible for selective oxidation are either reduced to V^{4+} or poisoned by carbonaceous deposits.

Let us now consider in more detail the nature of the main products (CO, CO_2, and the butene isomers) formed in a reducing atmosphere. The CO/CO_2 distribution during the course of the reaction is shown in Figs. 2a (PYRO catalyst) and 3b (PYRO.OX catalyst). It can be observed that CO and CO_2 selectivities are at first nearly identical. Then the CO_2 formation drops and CO becomes by far prevalent. These changes are rapid on the PYRO catalyst (Fig. 2a) but occur over a longer lapse of time on PYRO.OX catalyst (about 15 h, Fig. 2b). If one considers the usual simplified reaction scheme depicted in Fig. 8, the present observations strongly suggest that CO mainly comes from the oxidation of adsorbed butane and butenes whereas CO_2 is mainly produced by the overoxidation of MA. It is already known that under standard conditions, the selectivity for MA is mainly limited by the overoxidation of adsorbed MA (1).

According to Busca (42), the *n*-butane is first activated at C(2) giving rise to an adsorbed secondary butoxy group. These species can be further dehydrogenated oxidatively on the same carbon atom to the adsorbed ketone leading then to acetate species and CO*x*. Conversely, the selective way involves the formation of a mixture of adsorbed butenes which are normally rapidly converted to butadiene and eventually to MA, thanks to the acidic and oxidizing properties of the V–P–O catalysts. Butenes are evolved in the gas phase only on a surface that is nonreactive towards olefins, because the suitable selective oxidizing sites are lacking. Another reason could be that the surface is not acidic enough, like for Mg vanadates (43, 44).

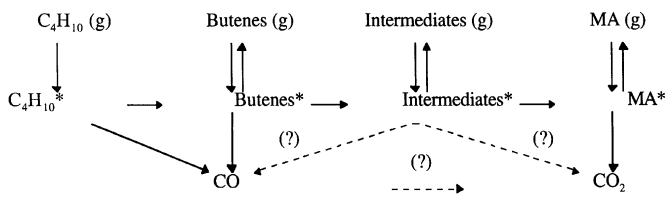

FIG. 8. Schematic representation of the reaction mechanism.

Besides the butenes isomers, 1,3-butadiene was detected after a few hours of reaction (but at a very low level, about 2.5%) for PYRO and PYRO.OX. The selectivity to 1-butene steadily increased with time whereas the selectivities to *cis*-2-butene and *trans*-2-butene followed similar changes and reached a maximum. It is known (14) that the formation of butene isomers is in line with the initial activation of *n*-butane by dissociation of a methylene C–H bond to form a secondary butyl radical. The further loss of a second hydrogen occurs either from a methyl group or from the other methylene group, and a statistical distribution of the isomers is then expected: 1-butene : *cis*-2-butene : *trans*-2-butene = 3 : 1 : 1. This distribution is actually observed provided the hydrogen loss is rapid and statistically occurs. Moreover, the residence time of adsorbed butenes should be very short (43, 44). Otherwise, the surface isomerization occurs and the equilibrium ratio 1 : 1 : 1.1 is observed (44).

It is interesting to look more closely at the type of distribution which is observed in the course of the reaction on PYRO and PYRO.OX catalysts. The experimental information is indeed in Figs. 3a and 5a, but the data are difficult to analyze in this respect. Therefore, in Figs. 3b and 5b, the different selectivities have been normalized with respect to the selectivity for *cis*-2-butene. Now it can be clearly seen that the general trends for PYRO (Fig. 3b) and PYRO.OX (5b) are similar with, however, again a longer time scale for PYRO.OX. In first approximation, the isomers distribution is at first almost statistical, then at equilibrium, and again statistical. Since there are no theoretical explanations for the higher selectivity for *trans*-2-butene compared to that of *cis*-2-butene, (1.5 : 1) instead of (1 : 1), this difference might well result from the experimental accuracy in the analysis of the reaction products. We therefore propose the following general analysis of the observed changes of selectivity with the course of the reaction under reducing conditions. At the beginning of the run, butenes were very quickly converted to butadiene and to further reaction intermediates which led to MA and CO*x* because of the presence of selective V^{5+} species. Furthermore, the overall selectivity for butenes was low (Figs .1b and 4b). As the catalyst was progressively reduced, butenes remained adsorbed for a longer time on the acidic sites insofar as oxidizing V^{5+} sites became scarce and an equilibrium ratio was observed. This step also coincides with the formation of a small amount of butadiene by oxydehydrogenation. Then the catalyst led to the formation of increasing amounts of butenes, especially 1-butene (Figs. 3a and 5a). Enough adsorption sites were then no longer available for the numerous butene molecules. The average residence time of individual butene molecules became again very small, and the statistical ratio was observed once more. Besides desorption, the adsorbed butenes produced in large amounts could only undergo cracking reactions leading to either carbonaceous deposits or

oxidation to CO and, to a small extent, dehydrogenation to butadiene.

Let us now come back to the complete inhibition of the selective oxidation route to MA which occurred when a low O_2/C_4H_{10} ratio was used (Figs. 1 and 4). We believe that under these conditions the total consumption of oxygen also plays a major role. In order to maintain the MA formation, it is crucial to avoid a total conversion of oxygen by all means, for example, by reducing the *n*-butane partial pressure or by changing the GHSV.

The reduction of the catalyst and the loss of MA selectivity was significantly delayed for the PYRO.OX catalyst. The reversibility of this reduction (reactivation of the catalyst) has been investigated. In order to look for the ability of the PYRO.OX catalyst to work under a large range of feed conditions, different steps of regeneration have been chosen. First, reducing–oxidizing–reducing treatments were performed on the PYRO.OX catalyst by changing the O_2/C_4 ratio, 0.6 in a first step, 12 in a second step, and again 0.6 in a third step.

Although the reduced PYRO.OX catalyst is selective with $O_2/C_4 = 12$, the catalyst is likely not reoxidized enough to form MA during the second fuel-rich step.

Therefore the catalyst was submitted to a treatment at 500°C under an oxygen flow for 2 h. Then this catalyst was able to work again with a ratio $O_2/C_4H_{10} = 0.6$, and the selectivity for MA was again fairly high: $S(\mathrm{MA}) = 41.7\%$. This last step shows that the catalytic properties of the PYRO catalyst can be largely recovered following a reactivation step under pure O_2.

This observation is in agreement with the redox character of this reaction also demonstrated by DuPont (20) using a recirculating solid reactor: the oxidation of *n*-butane is carried out in two steps. In the first step, the alkane is oxidized by the lattice oxygen of the catalyst (in the absence of gaseous oxygen), and in the second step the reduced catalyst is regenerated with air.

5. CONCLUSIONS

This study underlines the effects of the $O_2/n\text{-}C_4H_{10}$ ratio on the catalytic performance of a V–P–O (PYRO) catalyst. It shows that the solid, although selective toward maleic anhydride under standard feed conditions, $O_2/C_4H_{10} = 12$, is not adapted to work under the fuel-rich feed conditions ($O_2/C_4 = 0.6$) which prevail in the first layer of a membrane reactor. These reducing conditions lead to a rapid reduction of the catalyst surface, and the V^{5+} species are reduced to V^{4+} and masked and/or poisoned by carbonaceous deposits. Therefore, butenes and CO*x* formation are favored under reducing conditions.

An oxidizing pretreatment under pure O_2 at $T = 500$°C for 2 h allows the V–P–O catalyst to form MA for 15 h under fuel-rich conditions, thus delaying the reduction of the catalyst surface. This improvement of the catalyst properties must be related to the storage of lattice oxygen created by the O_2 treatment of the PYRO catalyst.

The butane activation would occur on single V^{4+} actives sites, and therefore the butane conversion is not very sensitive to the development of carbonaceous deposits occurring under reducing conditions. Conversely, ensembles of several surface V^{5+} species would be required to obtain the selective sites responsible for the crucial oxygen-insertion steps leading to MA. The presence of carbonaceous deposits originating from V^{4+} species reduces the access to V^{5+} sites. Consequently, butenes and CO*x* are again produced.

The highly reducing test conditions of reaction provide information on the mechanism of butenes and CO*x* formation. Results suggest that CO comes mainly from the oxidation of adsorbed butane and butenes whereas CO_2 is mainly produced by the overoxidation of MA. Concerning the butenes, their distribution in the gas phase depends on the acidity and the redox properties of the solid surface. Initially, when the selectivity to butenes was low, the C_4 isomer distribution was statistical, then it went to equilibrium (surface highly reduced), and finally again statistical (adsorption sites for butenes not available, CO formation).

Finally, this study shows that for highly reducing conditions ($O_2/C_4H_{10} = 0.6$) the key parameter is the oxygen consumption: the redox cycle does not operate when $C(O_2) = 100\%$. However, the reduction of the catalyst is reversible, which indicates that the active surface closely follows the redox influence of the reactant mixture. However, when strongly reduced, the catalyst requires a pure oxygen regeneration in order to be selective again toward MA under fuel-rich conditions ($O_2/C_4 = 0.6$).

This study provides important information which will have to be taken into account in the development of a membrane reactor presently in progress in our laboratory. It appears that enough oxygen should be co-fed with butane to limit nonselective catalysis at the inlet of the membrane reactor. The results also show that some catalyst development, such as improvement of the resistance of the active phase toward reduction, should be worthwhile when membrane reactors are considered. This will be the subject of a second paper dealing with the effect of doping a V–P–O catalyst working under oxygen-lean conditions.

ACKNOWLEDGMENTS

This work was conducted in the framework of the contract Brite BRPR-CT95-0046. The authors are indebted to the support of the European Community. We gratefully acknowledge Dr. P. Delichère and M. Brun for XPS analysis and Dr. A. Tuel and M. C. Durupty for NMR analysis.

REFERENCES

1. Centi, G., Trifiro, F., Ebner, J. B., and Franchetti, V. M., *Chem. Rev.* **88**, 55 (1988).

2. Cavani, F., and Trifiro, F., *Catalysis* **11**, 246 (1994).
3. Hodnett, B. K., *Catal. Rev. Sci. Eng.* **27**, 373 (1985).
4. Contractor, R. M., Bergna, H. E., Horowitz, H. S., Blackstone, C. M., Malone, B., Torardi, C. C., Griffiths, B., Chawdhry, U., and Sleight, A. W., *Catal. Today* **1**, 40 (1987).
5. Shimoda, T., Okuhara, T., and Misono, M., *Bull. Chem. Soc. Jpn.* **58**, 2163 (1985).
6. Busca, G., Cavani, F., Centi, G., and Trifiro, F., *J. Catal.* **99**, 400 (1986).
7. Moser, T. P., and Schrader, G., *J. Catal.* **92**, 216 (1985).
8. Duvauchelle, N., and Bordes, E., *Catal. Lett.* **57**, 81 (1999).
9. Bordes, E., *Catal. Today* **1**, 499 (1987).
10. Harrouch Batis, N., Batis, H., Ghorbel, A., Vedrine, J. C., and Volta, J. C., *J. Catal.* **128**, 248 (1991).
11. Centi, G., *Catal. Today* **16**, 1 (1993).
12. Abon, M., Béré, K. E., Tuel, A., and Delichère, P., *J. Catal.* **156**, 28 (1995).
13. Centi, G., Fornasari, G., and Trifiro, F., *J. Catal.* **89**, 44 (1984).
14. Overbeek, R. A., Ph.D. thesis, University of Utrecht, 1994.
15. Kwentus, G. K., European Patent Application 0189261 (1983).
16. Edwrads, R. C., and Udovich, C. A., U.S. Patent 4,649,205 (1987).
17. Contractor, R. M., European Patent Application 01899261 (1986).
18. Lerou, J., lecture presented at the second NIOK course on oxidation catalysis, Rolduc, Kerkrade, 6–9 June 1994.
19. Contractor, R. M., Granett, D. I., Horowitz, H. S., Bergna, H. E., Patience, G. S., Schwartz, J. T., and Sisler, G. M., *in* "New Developments in Selective Oxidation II," p. 233, 1994.
20. Centi, G., Fornasari, G., and Trifiro, F., *Ind. Eng. Chem. Prod. Res. Dev.* **24**, 32 (1985).
21. Hutchings, G., *Appl. Catal.* **72**, 1 (1991).
22. Harold, M. P., Lee, C., Burggraaf, A. J., Keizer, K., Zaspalis, V. T. and de Lange, R. S. A., *Mater. Res. Soc. Bull.* **34**, April 1994.
23. Coronas, J., Menéndez, M., and Santamaria, J., *Chem. Eng. Sci.* **24**, 4749 (1994).
24. Giroir-Fendler, A., Peureux, J., Mozzanega, H., and Dalmon, J. A., *Studies Surf. Sci. Catal.* **101A**, 127 (1996).
25. Aït-Lachgar, K., Abon, M., and Volta, J. C., *J. Catal.* **171**, 383 (1997).
26. Aït-Lachgar, K., Tuel, A., Brun, M., Hermann, J. M., Krafft, J. M., Martin, J. R., Volta, J. C., and Abon, M., *J. Catal.* **177**, 224 (1998).
27. Ben Abdelouahab, F., Olier, R., Guillaume, N., Lefebvre, F., and Volta, J. C., *J. Catal.* **134**, 151 (1992).
28. Johnson, J. W., Johnston, D. C., Jacobson, A. J., and Brody, J. F., *J. Am. Chem. Soc.* **106**, 8123 (1984).
29. Sananes, M. T., Tuel, A., and Volta, J. C., *J. Catal.* **145**, 251 (1994).
30. Joly, J. P., Mehier, C., Béré, K. E., and Abon, M., *Appl. Catal. A* **169**, 55 (1998).
31. Busca, G., Centi, G., and Trifiro, F., *Appl. Catal.* **25**, 265 (1986).
32. Bere, K. E., Gravelle, M., and Abon, M., *J. Chim. Phys.* **92**, 1521 (1995).
33. Bordes, E., and Contractor, R. M., *Topics Catal.* **3**, 365 (1996).
34. Schuurman, Y., and Gleaves, J. T., *Ind. Eng. Chem. Res.* **33**, 2935 (1994).
35. Coulston, G. W., Bare, S. R., Kung, H., Birkeland, K., Bethke, G. K., Harlow, R., and Herron, N., and Lee, P. L., *Science* **275**, 191 (1997).
36. Zhang-Lin, Y., Forissier, M., Sneeden, R. P., Vedrine, J. C., and Volta, J. C., *J. Catal.* **145**, 256 (1994).
37. Guliants, V. V., Benziger, J. B., Sundaresan, S., Wachs, I. E., Wachs, J. M., and Roberts, J. E., *Catal. Today* **28**, 275 (1996).
38. Cavani, F., Centi, G., Trifiro, F., and Grasselli, R. K., *Catal. Today* **3**, 185 (1988).
39. Ebner, J. R., and Thompson, M. R., *Catal. Today* **16**, 51 (1993).
40. Agaskar, P. A., Decaul, L., and Grasselli, R. K., *Catal. Lett.* **23**, 339 (1994).
41. Cavani, F., and Trifiro, F., *Appl. Catal. A* **157**, 195 (1997).
42. Busca, G., *Catal. Today* **27**, 457 (1996).
43. Chaar, M. A., Patel, D., Kung, M. C., and Kung, H. H., *J. Catal.* **105**, 483 (1987).
44. Blasco, T., Lopez Nieto, J. M., Dejoz, A., and Vasquez, M. I., *J. Catal.* **157**, 271 (1995).